Generalized model for ultrafast laser induced electron emission from a metal tip

L. K. Ang and M. Pant

Citation: Phys. Plasmas **20**, 056705 (2013); doi: 10.1063/1.4803086
View online: http://dx.doi.org/10.1063/1.4803086
View Table of Contents: http://pop.aip.org/resource/1/PHPAEN/v20/i5
Published by the American Institute of Physics.

Generalized model for ultrafast laser induced electron emission from a metal tip[a)]

L. K. Ang[1,2,b)] and M. Pant[1]
[1]*Singapore University of Technology and Design, Singapore 138682*
[2]*School of Electrical and Electronic Engineering, Nanyang Technological University, Singapore 639798*

(Received 14 December 2012; accepted 21 February 2013; published online 3 May 2013)

In this paper, we will present a brief review of the recently developed non-equilibrium heating and time dependent tunneling model to study the dynamic processes in using an ultrafast laser to induce electron emission from a metallic tip ranging from the multiphoton to the optical tunneling regime. Due to the short time scale of the ultrafast laser pulse, the lattice is found to be in a non-equilibrium condition and a single temperature model is no longer valid. The ultrafast laser heating enhances the electron emission through both the multiphoton and optical tunneling processes rather than over-barrier emission due to thermal heating. The paper is focused on the methodology of how these two effects (non-equilibrium heating and time-dependent tunneling) are combined in a self-consistent model. The model shows a smooth transition of the emitted charge as a function of laser field, ranging from the multiphoton emission regime at low laser field to the optical tunneling regime at high laser field. The paper will conclude with some discussion of future work.
 [http://dx.doi.org/10.1063/1.4803086]

INTRODUCTION

For a metal with a work function Φ_m, N photons must be absorbed by an electron to be emitted from the surface by overcoming the surface barrier with an energy $N \times h\nu > \Phi_m$, where h is the Planck constant and ν is the frequency of light. This emission process, known as multiphoton emission, can be considered as the generalized Einstein photoelectric effect. The first quantitative model to calculate electron photoemission by multiphoton absorption was the Fowler-Dubridge (FD) law[1–3] in the 1930s.

Another mechanism for electron emission is by quantum mechanical tunneling through the barrier, which is known as field emission and is described by the Fowler-Nordheim (FN) law proposed in 1928 (Ref. 4) when a sufficiently high DC electric field is applied to suppress the barrier so that the tunneling process can become important.

The third mechanism for electron emission is thermionic emission in which the temperature of a cathode increases due to heating, and it is described by the Richardson-Laue-Dushman (RLD) law[5] proposed in 1921. Since these pioneering works, there have been many extensions and improvements to all the three emission models described above. A good overview can be found in a recent review by Jensen.[6] In particular, all three emission mechanisms can be combined in a generalized model.[7]

In 1965, Keldysh[8] presented a model to study the ionization of atoms to release bounded electrons. Based on the proposed Keldysh parameter $\gamma = \omega\sqrt{2em\Phi_m}/eF$, where ω and F are, respectively, the frequency and field strength of laser light, and Φ_m is the ionization potential, the emission mechanism can be identified. In the regime of multiphoton emission defined by $\gamma \gg 1$ (small F), the ionization process is dominated by the absorption of 1 or more photons from the laser field. In the other limit of $\gamma \ll 1$ (large F), the electrons are released by tunneling through the barrier under the influence of the laser field, which is known as optical field emission or the optical tunneling regime.

Recently, there has been an interest in using ultrafast laser-induced electron emission from a DC-biased sharp metallic tip[9–17] to create ultrafast electron bunches for many applications. While the emission mechanism is well known in both $\gamma \gg 1$ and $\gamma \ll 1$ regimes, most current experiments are conducted in the transition regime between $\gamma = 1$ and 10, in which the emission mechanism is hard to pin down. Pioneering experimental works by two research groups have claimed different emission mechanisms, such as optical field emission at $\gamma = 3$ to 9 for tungsten[9] and multiphoton emission at $\gamma = 4$ for gold.[10] Another group has reported multiphoton absorption followed by over-barrier emission ($\gamma = 3$ to 4).[11] Subsequent works include further investigation in the strong field regime with the discovery of new physics, such as strong field photoemission,[12,13] above threshold photoemission,[14] attosecond control of electron emission from sharp metal tips,[15] quiver motion,[16] and using hafnium carbide tips.[17]

In most studies, there is one important aspect of the laser-metal interaction that has been ignored, which is the heating of the metal by the ultrafast laser. At the ultrafast time scale, the traditional heating model used for long pulse laser-metal interaction is no longer valid as the pulse length of the ultrafast laser is shorter than the electron-phonon relaxation time in metals. In 2008, we developed a non-equilibrium heating model by solving microscopic kinetic equations to include electron-electron and electron-phonon collisions.[18] From the calculated time-dependent

[a)]Paper CI2 2, Bull. Am. Phys. Soc. **57**, 70 (2012).
[b)]Invited speaker. Author to whom correspondence should be addressed. Electronic mail: ricky_ang@sutd.edu.sg

non-equilibrium electron distribution, we calculate the emitted current density by using the WKBJ method to obtain the tunneling coefficient. It is found that this model is able to explain prior experimental findings[9,11] rather well without assuming optical field emission (see Figs. 4 and 5 in Ref. 18). Our model was also later confirmed by an independent experimental measurement of the electron energy distribution.[19]

As mentioned before, the recent experiments were conducted in the regime of $\gamma = 1$ to 10, where both multiphoton and optical tunneling cannot be ignored. In particular, an experiment by Ropers' group in 2010 (Ref. 12) has shown a smooth transition from the multiphoton to the optical tunneling regime by using a 30 fs laser at 830 nm impinging on a gold tip, and it was roughly estimated that the transition is at about $\gamma = 2$ with a local laser field of 9 to 10 V/nm. To explain this transition, we have recently constructed a time-dependent quantum tunneling model[20] with the assumption that the electrons are emitted from the Fermi energy level (single energy model without heating). From our model, we are able to determine a critical Keldysh parameter which characterizes the onset of the optical tunneling regime and is only dependent on the work function of the material. In the multiphoton regime, we also found that the number of photons required may be reduced at ultrashort laser pulselengths due to the uncertainty principle. For example, it was predicted that 3-photon electron emission will be reduced to 2-photon if the pulse length is reduced from 20 fs to 8 fs. The phase dependence of the laser is found to be important only in the optical tunneling regime. All these findings can be found in Figs. 1 to 5 in Ref. 20.

It is clear that a combination of non-equilibrium heating and time-dependent tunneling is required in order to have a better model for the description of ultrafast laser induced electron emission. Recently, we have constructed such a time-dependent and non-equilibrium model, which also includes the effect of the laser field gradient.[21] Using this model, we are able to discover new phenomena that were absent from prior models and provide better agreement with experiments. The new findings include resonant emission of electrons at certain energies when the barrier height is equal to a multiple of photon energy. In the multiphoton regime, the generalized Einstein photoelectric effect is no longer valid, and electrons are emitted mostly from slightly below the Fermi energy level. The model also gives better agreement with experiment. These results can be found in Ref. 21.

In this paper, we will provide a complete description of the methodology used in our recently developed model including both the time-dependent dynamic laser-heating and tunneling processes. This model can be considered as a generalized model of ultrafast laser induced electron emission as it has included all 3 emission processes (thermal, photoemission, and tunneling). Note that our model has ignored space charge effects in both the quantum regime[22,23] and the ultrafast pulse limit,[24] which may be important due to recent results.[25,26] The extension of our model to include self-consistent space charge effects is currently in progress.

In Sec. II, we will present the description of our model. Lastly, we will conclude the paper with some remarks and proposals for future work.

DESCRIPTION OF THE MODEL

The system consists of a laser shining on a metallic tip with the electric field of the laser aligned perpendicular to the metal surface. The electric field of the laser at the surface of the metal is described by

$$F_{laser} = F_0 \exp\left(-2\ln 2\frac{(t-t_0)^2}{\tau^2}\right)\cos(\omega(t-t_0)+\phi), \quad (1)$$

with wavelength λ, pulsewidth τ, peak envelope field F_0, and phase angle ϕ. t_0 is the middle (or peak) of the laser pulse. The tip radius is r_0 and it is biased with a DC field F_{DC}. It should be noted that the field decays spatially because of the radius of curvature of the tip which will be described later. Note that F_{laser} in Eq. (1) is the field at the surface of the metal (at $x = 0$), and F_0 has included an arbitrary field enhancement.

In this paper, the default values of parameters are $\lambda = 800$ nm, $\tau = 20$ fs, $F_0 = 3$ V/nm, $\phi = 0$, $F_{DC} = 0.2$ V/nm, $t_0 = 40$ fs, and $r_0 = 20$ nm. Unless specified, the metal is tungsten with work function $\Phi_m = 4.4$ eV and the Fermi level $E_F = 5.78$ eV with respect to the metal potential energy.

The model consists of two parts. First, time-dependent kinetic equations are used to determine the effect of non-equilibrium heating on the electron energy distribution inside the metal. This distribution is used to determine the time dependent electron energy in different transmission channels, which will act as an input to the second part of the model: the time-dependent quantum model in order to calculate the emitted current density across different channels. The product of current and electron density is then integrated to give the total current as a function of time.

In the first part of the model, time-dependent kinetic equations are used to determine the distribution function of the electron gas $f(k)$ and the phonon gas $g(q)$, where k and q are the electron and phonon wavevectors. Here, we will not repeat the formulation which has been published before.[18] Using the time-dependent kinetic equations, we calculate the time-varying electron energy distribution function under the excitation of the ultrafast laser pulse given by Eq. (1).

In Fig. 1(a), the electron energy distribution function $f(E_e)$ after laser excitation is plotted at different times (within and after the 20 fs, 800 nm laser pulse) as a function of the electron energy $E_e = \hbar^2 k^2/2m$. Before the excitation, the electron energies are described by a Fermi-Dirac distribution function at 300 K at $t = 0$. The laser excitation or heating creates a strong nonequilibrium distribution, characterized by a steplike profile with an increase in E_e equal to the photon energy of 1.553 eV (800 nm). For example, the first, second, and third steps correspond to 1, 2, and 3 photon absorption, respectively. From the figure, we see that the excitation (or heating) of the laser pulse is maximized at around the peak of the laser pulse at $t = t_0 = 40$ fs. The steplike characteristic is dominant from $t = 20$ to 60 fs. After the

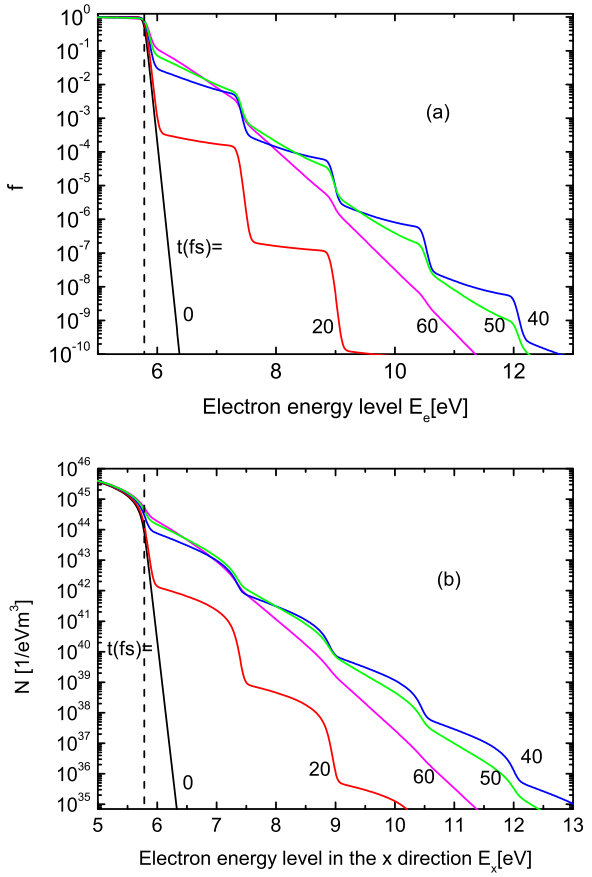

FIG. 1. Evolution of (a) electron energy distribution function f and (b) electron density function $N(E_x)$ with default parameters. Vertical dashed lines represent the Fermi level $E_F = 5.78$ eV.

peak ($t = 40$ to 60 fs), the electrons start cooling down by losing energy to the lattice and the step-like behavior starts smoothing out due to the e-e and e-p collisions. After $t = 60$ fs, the distribution reaches a new quasi-equilibrium state with a new Fermi-Dirac distribution at a higher temperature >300 K.

In order to determine the emitted current, the electron density is required to be calculated as a function of energy in the x direction E_x, i.e., perpendicular to the metal tip. The distribution as a function of E_x is found by integrating over phase space given by the formula

$$N(E_x, t)dE_x = \frac{(me/2)^{3/2}dE_x}{\pi^2\hbar^3\sqrt{E_x}} \int_{E_x}^{\infty} f(E_e)dE_e. \qquad (2)$$

Fig. 1(b) shows the corresponding time-dependent $N(E_x, t)$. Compared to Fig. 1(a), Fig. 1(b) also shows similar behavior with peak deviation at $t = t_0 = 40$ fs, and the step-like behavior is dominant from $t = 20$ to 60 fs.

Next, the non-equilibrium electron energy in different transmission channels is determined based on the change of different electron density levels. The initial energy E_0 of each channel can be used to represent different transmission channels. The electron density in a channel represented by E_0 is defined as $N(E_0)$. Hence, its energy at a future time can be represented as $E_x(E_0, t) = N^{-1}[N(E_0)]$, where $N(E_0)$ has been calculated as shown in Fig. 1(b). The evolution of the energies of different transmission channels (or different E_0) with various parameters is shown in Fig. 2. Results shown in Fig. 2(a) have assumed default parameters. From the figure, we see that the energy increases in steps equal to the photon energy before the peak of the laser pulse as $t = t_0 = 40$ fs (indicated by the vertical dashed lines) and the step-like behaviour is smoothed gently after $t = 40$ fs due to cooling.

When τ is reduced to 8 fs [see Fig. 2(b)], the same behavior repeats, except that the heating and cooling take place over a shorter time scale as expected. When the wavelength is reduced to 550 nm [see Fig. 2(c)], the steps in the graph become larger because of the increase in photon energy (smaller wavelength of 550 nm $<$ 800 nm). When F_0 is increased to 30 V/nm [see Fig. 2(d)], the increase in

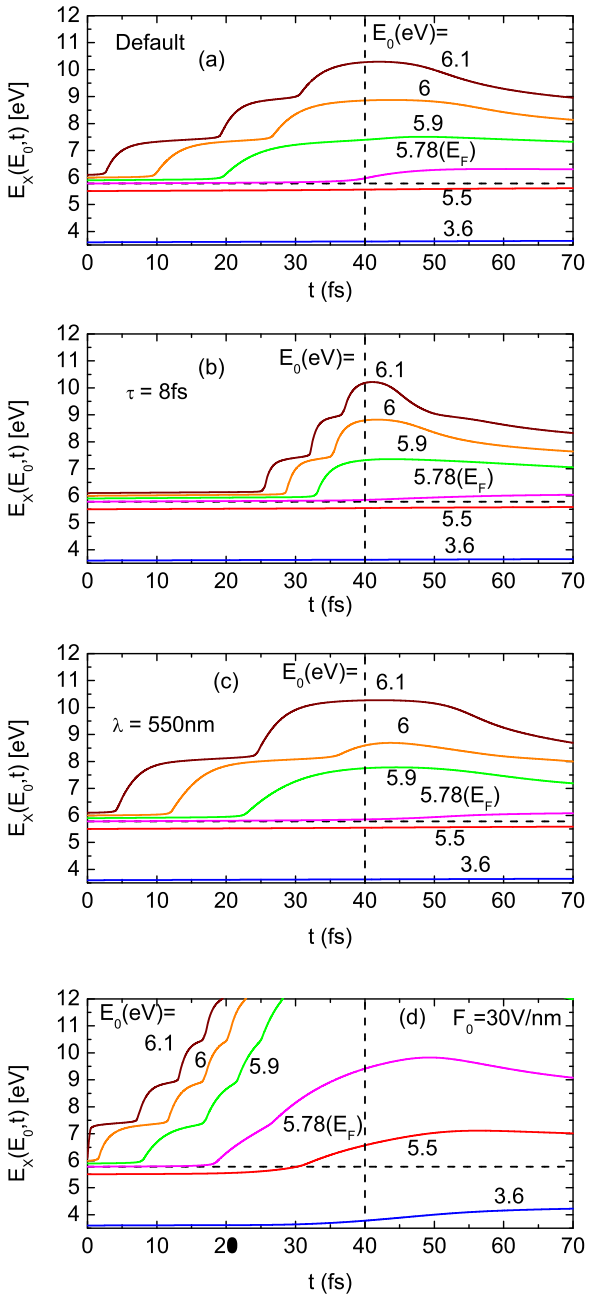

FIG. 2. Evolution of electron energy in different transmission channels with varying laser parameters. Vertical dashed lines represent $t_0 = 40$ fs and horizontal dashed lines represent the fermi level $E_F = 5.78$ eV.

electron energy becomes much larger. However, it should be noted that the increase in tunneling current is much more significant than the heating effect at high fields.[21] Note that tunneling effects and over barrier emission are not reflected in Figs. 1 and 2 as they are implemented in the time-dependent quantum simulation which is the second part of the model (see below).

From the obtained $E_x(E_0,t)$ (as shown in Fig. 2), we solve the time-dependent Schrödinger equation (TDSE) for each transmission channel at $E_x(E_0,t)$. In the TDSE, we have the following surface potential barrier given by:

$$U(x,t) = E_{vac} - \frac{e^2}{16\pi\epsilon_0(x+x_0)} - e\left[F_{DC}x + F_0 x \times \exp\left(-2\ln 2\frac{(t-t_0)^2}{\tau^2}\right)\cos(\omega(t-t_0)+\phi)\right] \times \left[(1/2)\frac{r_0}{x}\left(1-\frac{1}{(x/r_0+1)^2}\right)\right], \quad (3)$$

where $E_{vac} = \Phi_m + E_F$ is the vacuum energy (= 10.18 eV for tungsten) and the metal-vacuum interface is at $x = 0$. The second term is the classical image charge term and we have $x_0 = e/[16\pi\epsilon_0 E_{vac}]$ in order to implement the continuity of the potential energy. The last term in the equation represents the effect of the field gradient which causes the field to decay as $F(x) \approx F \times (r_0/(x+r_0))^3$. In the derivation of the third term, we have assumed that the beam waist is large as compared to the barrier width and the tip has a large geometric field enhancement.[16] The integration of this term will account for the contribution of the laser field to the potential energy which is $-\int_0^x F \times (r_0/(x+r_0))^3 dx = -x \times F(r_0/2x)[1 - 1/(x/r_0+1)^2]$. Note that this term is only important for a very small tip with radius $r_0 < 40$ nm [see Fig. 6 in Ref. 21].

First, the initial wavefunction Ψ_0 for each transmission channel is found by solving the time independent Schrödinger equation with $F_{DC} = F_0 = 0$. Based on the continuity of the wavefunction at x = 0 and the requirement that the wavefunction must decay at infinity, we have

$$\Psi_0(x<0) = C_1\sin(k_m x) + C_2\cos(k_m x)$$
$$\Psi_0(x>0) = C_3 W_{a/2\sqrt{b},-1/2}(2\sqrt{b}(x+x_0)), \quad (4)$$

where $k_m = \sqrt{2mE_0}/\hbar$, $W_{k,m}(x)$ is the Whittaker W function, $a = e^2 m/(8\hbar^2\pi\epsilon_0)$ and $b = 2(E_{vac} - E_0)/\hbar^2$.

The variation in E_x is implemented by changing the potential energy inside the metal. The fact that this does indeed cause the desired effect was numerically verified and we found that an increase in the potential energy inside the metal causes the same effect as decreasing the work function by changing the initial wavefunction. Physically, it can be seen that increasing the potential energy lowers the barrier and effectively increases E_x.

The time-dependent current density $J[E_x(E_0,t,t)]$ of each channel is then calculated at x = 2 nm from the wave function solved from the TDSE model. The contribution of each energy level to the total current at a particular time, also called the spectral current density, is defined as $N(E_x)J(E_x,t)$ and is plotted in Fig. 3. For a fair comparison, the times plotted in Fig. 3 all correspond to laser peaks. It is found that the current at $t = 48$ fs is found to be larger than the current at $t = 40$ fs because of the finite time required by the electron to tunnel through the barrier and to reach x = 2 nm. The heating process also causes a delay in the peak emission which is discussed later. The peaks move to lower E_x after 40 fs as was shown in Fig. 2 as well due to cooling.

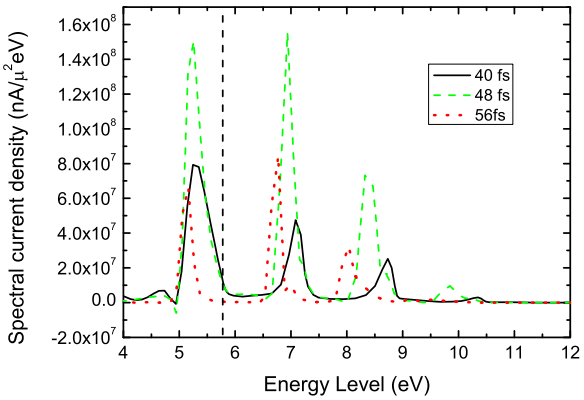

FIG. 3. Spectral current density $N(E_x)J(E_x,t)$ at different instants with default parameters.

Finally, we have also benchmarked our model by turning off the laser field ($F_L = 0$) and compared our results with the classical FN law in the range of DC field from 2.5 to 4 V/nm, which shows reasonable agreement.

DISCUSSION AND FUTURE WORK

In this section, we present the emission characteristics as predicted by our model. We observe a number of significant differences between our simulations and previous single energy models which assume emission from the Fermi level and ignore heating. These differences are discussed in Figures 4 and 5. A further discussion is also provided in a coming publication.[21] Some earlier reported results have been summarized in the introduction section.

Figure 4 shows the total current $J_{tot}(t) = \int N(E_x)J(E_x,t)dE_x$ as a function of time with different parameter values. In the black dashed line, $f(E_e)$ is held constant at the Fermi-Dirac distribution in order to ignore the effects of heating. Heating is found to cause an increase in current as seen on comparing the solid and dashed black lines. Unlike single energy models,[20] the peak photocurrent depends on the pulsewidth. Finally, when F_0 is increased sufficiently such that the emission enters the optical tunneling regime (Fig. 4(b)), the relative importance of heating decreases and the peaks can be found to occur earlier than in Fig. 4(a).

The same effect can also be observed in Fig. 5 where we plot the total photoemitted charge σ (calculated by integrating J_{tot} over time) as a function of F_0 for different models. Although an increase in laser intensity increases electron energy (as seen in Fig. 2(d)), the relative impact on tunneling is much larger. At high fields, a significant number of electrons at lower energies can tunnel through the energy

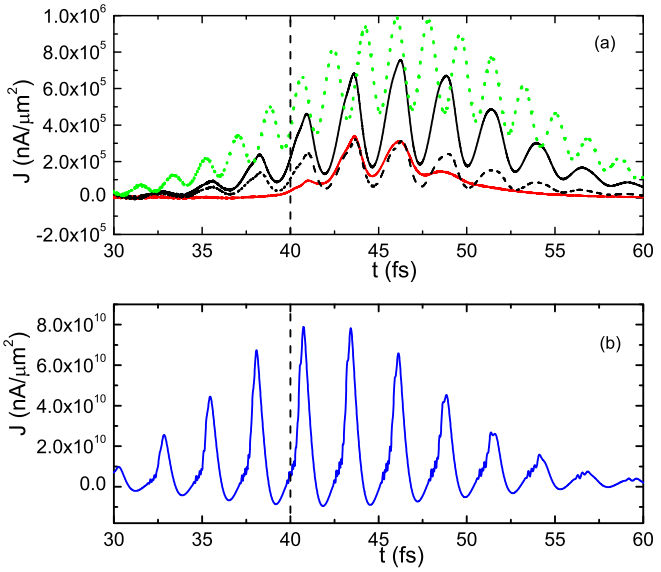

FIG. 4. Plot of current density J as a function of time with different parameter values: (a) default parameters (black solid line), default parameters with no heating (black dashed line), $\lambda = 550$ nm (green dotted line), $\tau = 8$ fs and (b) $F_0 = 30$ V/nm. The vertical dashed line is the middle of the laser pulse at $t_0 = 40$ fs.

barrier[21] and the relative impact of heating becomes smaller. This can be seen by comparing the heating (black solid) and no-heating (green dashed) lines in Fig. 5 which converge at high F_0. It should be noted that Fig. 5 is plotted on a logarithmic scale and the difference between the two lines is quite significant. The smooth transition shown in the figure agrees with experimental observations[12] for which the single energy model shows unphysical fluctuations at high $F_0 > 10$ V/nm (red dashed line).

In the figure, we also plot a case of higher Fermi energy level ($E_F = 2 \times 5.78\,\text{eV} = 11.56\,\text{eV}$) in symbols to see the effect of the Fermi energy level. The comparison shows that the higher Fermi energy case (symbols) has smaller σ compared to the lower Fermi energy case (solid). The difference is about a factor of $\sqrt{2}$ lower, which is due to the $1/\sqrt{E_x}$ factor in Eq. (2). The difference is, however, reduced at high

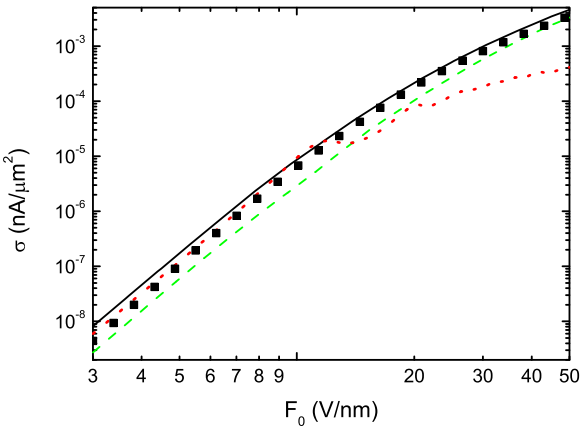

FIG. 5. Plot of F_0 vs emitted charge density σ with default parameters as calculated by the single energy model (red dotted line), multiple energy model with no heating (green dashed line), and the combined model (black solid line) The symbols are the combined model but at higher (2 times) fermi energy of $E_F = 2 \times 5.78\,\text{eV} = 11.56\,\text{eV}$.

field $F > 10$ V/nm where optical field emission is more dominant.

There are certain aspects of the model that can be improved in the future that we will discuss briefly below. Space charge effects have been ignored in the model and it would be interesting to investigate whether the emission is in the space charge limited regime at high laser fields. Furthermore, in order to simplify the integrals in the kinetic equations, the heating was assumed to be isotropic. These assumptions tend to slightly overestimate the impact of heating. Another aspect is the lack of spatial dependence in the heating model. The classical image charge term used in Eq. (3) is similar to the one used in previous studies.[9,20] A time dependent image charge term could be introduced in future work to further improve the accuracy of the model. The model also ignores how the field enhancement factor may behave at the ultrafast time scale.

It is important to note that the effect of nonequilibrium excitation of the electron distribution in metals had been reported in an earlier phenomenological theory of nonlinear multiphoton electron emission.[27] However, their treatment was very different from our model, where they had adopted a two-temperature like approach in solving the coupled thermal equations. In our model, we have solved Boltzmann equations to account for the energy transfer between electrons and phonons and have ignored completely the thermal conduction and diffusion on the consideration that these effects occur at a much longer time scale. Similarly, the normal heating of the laser[28] and absorption due to roughness[29] are also not considered based on the same argument of the time-scale difference. Finally, our model is essentially a 1D model even though we have included an effective enhancement of the electric field due to the field gradient near the tip [see last term in Eq. (4)]. This simplified model will not be able to account for some of the complicated and interesting dynamics of electrons near the tip, which have been reported recently, such as electron steering[30] and electron rescattering.[31] It would also be interesting to have a consistent model that is able to show the transition from ultrafast time scale to a longer time scale which may recover the traditional FD law for ps laser multiphoton emission.[1–3]

In this paper, we have presented the details of our model, which combines the effects of non-equilibrium heating and time dependent quantum tunneling that have been studied in isolation in previous studies. Our model has shown that both effects are significant in femtosecond laser induced photoemission.[18,20,21] The model will be useful for further developments to include new effects discovered recently such as strong field photoemission,[12,13] above threshold photoemission,[14] attosecond control of electron emission from sharp metal tips,[15] quiver motion,[16] electron steering[30] and electron rescattering.[31]

ACKNOWLEDGMENTS

This work was supported by Singapore MOE grant (2008-T2-01-033), SUTD (SRG EPD 2011 014) and SUTD-MIT IDC grant (IDG21200106 and IDD21200103). L. K. Ang would like to acknowledge the support of USA

AFOSR-AOARD grant (11-4069) and USA ONR-Global grant (N62909-10-1-7135).

[1]R. H. Fowler, Phys. Rev. **38**, 45 (1931).
[2]L. A. DuBridge, Phys. Rev. **39**, 108 (1932).
[3]L. A. DuBridge, Phys. Rev. **43**, 727 (1933).
[4]R. H. Fowler and L. Nordheim, Proc. R. Soc. London, Ser. A **119**, 173 (1928).
[5]O. W. Richardson, *The Emission of Electricity from Hot Bodies* (Longmans, Green, New York, 1921).
[6]K. L. Jensen, *Advances in Imaging and Electron Physics*, Vol. 149 (Elsevier, 2007).
[7]K. L. Jensen, P. G. O'Shea, and D. W. Feldman, Appl. Phys. Lett. **81**, 3867 (2002).
[8]L. V. Keldysh, Sov. Phys. JETP **20**, 1307 (1965).
[9]P. Hommelhoff, C. Kealhofer, and M. A. Kasevich, Phys. Rev. Lett. **97**, 247402 (2006).
[10]C. Ropers, D. R. Solli, C. P. Schulz, C. Lienau, and T. Elsaesser, Phys. Rev. Lett. **98**, 043907 (2007).
[11]B. Barwick, C. Corder, J. Strohaber, N. Chandler-Smith, C. Uiterwaal, and H. Batelaan, New J. Phys. **9**, 142 (2007).
[12]R. Bormann, M. Gulde, A. Weismann, S. V. Yalunin, and C. Ropers, Phys. Rev. Lett. **105**, 147601 (2010).
[13]S. V. Yalunin, M. Gulde, and C. Ropers, Phys. Rev. B **84**, 195426 (2011).
[14]M. Schenk, M. Krüger, and P. Hommelhoff, Phys. Rev. Lett. **105**, 257601 (2010).
[15]M. Krüger, M. Schenk, and P. Hommelhoff, Nature **475**, 78 (2011).
[16]G. Herink, D. R. Solli, M. Gulde, and C. Ropers, Nature **483**, 190 (2012).
[17]C. Kealhofer, S. M. Foreman, S. Gerlich, and M. A. Kasevich, Phys. Rev. B. **86**, 035405 (2012).
[18]L. Wu and L. K. Ang, Phys. Rev. B **78**, 224112 (2008).
[19]H. Yanagisawa, M. Hengsberger, D. Leuenberger, M. Klockner, C. Hafner, T. Greber, and J. Osterwalder, Phys. Rev. Lett. **107**, 087601 (2011).
[20]M. Pant and L. K. Ang, Phys. Rev. B. **86**, 045423 (2012).
[21]M. Pant and L. K. Ang, "Time-dependent quantum tunneling and non-equilibrium heating model for the generalized Einstein photoelectric effect" (to be published).
[22]L. K. Ang, T. J. T. Kwan, and Y. Y. Lau, Phys. Rev. Lett. **91**, 208303 (2003).
[23]L. K. Ang, W. S. Koh, Y. Y. Lau, and T. J. T. Kwan, Phys. Plasmas **13**, 056701 (2006).
[24]L. K. Ang and P. Zhang, Phys. Rev. Lett. **98**, 164802 (2007).
[25]W. Wendelen, D. Autrique, and A. Bogaerts, Appl. Phys. Lett. **96**, 051121 (2010).
[26]W. Wendelen, B. Y. Mueller, D. Autrique, B. Rethfeld, and A. Bogaerts, J. Appl. Phys. **111**, 113110 (2012).
[27]J. Girardeau-Montaut and C. Girardeau-Montaut, Phys Rev. B **51**, 13560 (1995).
[28]J. H. Bechtel, J. Appl. Phys. **46**, 1585 (1975).
[29]L. K. Ang, Y. Y. Lau, R. M. Gilgenbach, and H. L. Spindler, Appl. Phys. Lett. **70**, 696 (1997).
[30]D. J. Park, B. Piglosiewicz, S. Schmidt, H. Kollmann, M. Mascheck, and C. Lienau, Phys. Rev. Lett. **109**, 244803 (2012).
[31]G. Wachter, C. Lemell, J. Burgdörfer, M. Schenk, M. Krüger, and P. Hommelhoff, Phys. Rev. B **86**, 035402 (2012).